García Martínez, A.; Piqueras, P.; Monsalve-Serrano, J.; Lago-Sari, R. (2018). Sizing a conventional diesel oxidation catalyst to be used for RCCI combustion under real driving conditions. Applied Thermal Engineering. 140:62-72. https://doi.org/10.1016/j.applthermaleng.2018.05.043

Sizing a conventional diesel oxidation catalyst to be used for RCCI combustion under real driving conditions

Antonio García*, Pedro Piqueras, Javier Monsalve-Serrano and Rafael Lago Sari

CMT - Motores Térmicos, Universitat Politècnica de València, Camino de Vera s/n, 46022 Valencia, Spain

Applied Thermal Engineering
Volume 140, 25 July 2018, Pages 62–72
https://doi.org/10.1016/j.applthermaleng.2018.05.043

Corresponding author (*):
Dr. Antonio García Martínez (angarma8@mot.upv.es)
Phone: +34 963876574
Fax: +34 963876574

Abstract

Reactivity controlled compression ignition (RCCI) combustion has demonstrated to be able to avoid the NOx-soot trade-off appearing during conventional diesel combustion (CDC), with similar or better thermal efficiency than CDC under a wide variety of engine platforms. However, a major challenge of this concept comes from the high hydrocarbon (HC) and carbon monoxide (CO) emission levels, which are orders of magnitude greater than CDC, and similar to those of port fuel injected (PFI) gasoline engines. The high HC and CO emissions levels combined with the low exhaust temperatures during RCCI operation could present a challenge for the current exhaust aftertreatment technologies.

The objective of this work is to evaluate the potential of a conventional diesel oxidation catalyst (DOC) for light-duty diesel engines when operating under dual-fuel RCCI diesel-gasoline combustion and to define its necessary size to accomplish with the current emissions standards. For this purpose, a 1-D model has been developed and calibrated through gas emissions measurements upstream and downstream the DOC under different engine steady-state conditions. After that, the DOC response in transient conditions has been evaluated by means of vehicle systems simulations under different driving cycles representative of the homologation procedures currently in force around the world. The results show that the HC and CO levels at the DOC outlet are unacceptable considering the different emissions regulations. By this reason, a dedicated study to define the DOC size needed to accomplish the different emissions standards is carried out. The results suggest that, the DOC volume needed to fulfill the type approval regulation limits ranges from four to six times the original volume.

Keywords

Reactivity controlled compression ignition; Dual-fuel combustion; Aftertreatment; Catalyst; Emissions

1. Introduction

Compression ignition (CI) engines are widely used worldwide because they combine high efficiency with moderate engine-out emissions [1]. However, the evolution of the limits imposed by the emissions standards have forced the manufacturers to include aftertreatment equipment to reduce the emissions before being emitted to the atmosphere [2][3].

The most harmful emissions from diesel engines are the nitrogen oxides (NOx) and soot. Moreover, it exists a trade-off when operating under conventional diesel combustion (CDC) by which reducing one pollutant, the other increases [4]. Thus, current automotive diesel engines require using a selective catalyst reduction (SCR) to reduce NOx, together with a diesel particulate filter (DPF) for soot emissions [5][6]. The addition of these elements at the exhaust line implies an increase of the production costs due to the increased complexity level as well as the operation costs due to the maintenance required and consumption of exhaust fluids needed for their operation (urea injection upwards the SCR and diesel fuel for passive DPF regenerations) [7][8]. Additionally, these systems generate an extra back pressure at the exhaust manifold, which reduces the fuel-to-work conversion efficiency and increases the fuel consumption [9].

During the past decades, alternative combustion strategies for compression ignition engines are being developed as a method to minimize the aftertreatment requirements to meet the current standards [10]. In this sense, the low temperature combustion (LTC) strategies are investigated to provide the benefits of CDC in terms of efficiency and performance whereas the engine-out NOx and soot emissions are reduced simultaneously [11][12]. This reduction is possible by operating with highly diluted fuel-air mixtures at the combustion chamber, which also leads to increase the fuel-air mixing time before the start of combustion [13][14]. In terms of efficiency, the most important factor that allows reaching such a high efficiency is the reduction of combustion duration and heat transfer [15].

Nowadays, the most promising LTC concept in terms of efficiency, emissions and engine load operating range capabilities is the dual-fuel concept so-called reactivity controlled compression ignition (RCCI) [16]. The RCCI concept relies on using two fuels of different reactivity injected by separated injection systems [17]. The high reactivity fuel (HRF) is directly injected into the cylinder, while the low reactivity fuel (LRF) is injected through the intake port [18]. As shown in previous studies, to achieve a highly efficient RCCI operation with low emissions, the major part of the total injected fuel should be LRF, while the HRF is used to trigger the combustion process [19][20]. Moreover, the HRF has a key role on the in-cylinder reactivity stratification, so that the HRF injection settings are one of the most important parameters for the combustion process development [21]. This reactivity gradient inside the cylinder allows a more sequential autoignition than other LTC concepts [22], which reduces the pressure gradients and enables extending the operating range.

The potential of the RCCI concept has been recently demonstrated in different engine platforms: single-cylinder [23], multi-cylinder [24], heavy-duty [25], medium-duty [26] and light-duty diesel engines [27] operating with low [28], medium [29] and high [30] compression ratios (CR). These works conclude that RCCI is able to achieve NOx levels below the limits proposed by the emissions regulations, together with ultra-low soot

emissions without the need for aftertreatment devices [31]. Nonetheless, RCCI still has several challenges that restrict its operating range and limit its practical application. By this reason, the dual-mode concept is being extensively investigated in the recent years [32][33]. This concept is based on switching to another combustion regime, typically CDC, to complete the engine map region in which the RCCI operation becomes critical either for excessive HC and CO emissions (low load) or maximum pressure rise rates (MPRR) and maximum in-cylinder pressures (high load) [34].

NOx and soot emissions with the dual-mode RCCI/CDC have been found substantially improved versus single CDC operation. However, the HC and CO emissions levels with this concept still are orders of magnitude greater than with CDC [35]. The major part of the HC and CO emissions are emitted during the operation in the RCCI portion of the map. Considering the low exhaust temperatures found during RCCI operation, these high levels of HC and CO could present a challenge for the diesel oxidation catalyst. Moreover, the gasoline to diesel ratio varies across the RCCI engine map, and therefore the chemical composition of the unburned compounds in the exhaust stream also changes.

The objective of this work is to evaluate the response of an automotive diesel oxidation catalyst when used for RCCI combustion as well as to define its size to accomplish with different emissions regulations. For this purpose, experimental tests have been done in a single-cylinder engine using diesel-gasoline as fuel combination. A 1-D model has been developed and calibrated through gas emissions measurements upstream and downstream the DOC under different engine steady-state conditions. After that, the DOC response in transient conditions has been evaluated by means of vehicle systems simulations under different driving cycles. In particular, the Real Driving Emissions (RDE) cycle, Worldwide harmonized Light vehicles Test Cycle (WLTC), Federal Test Procedure (FTP-75) and JC08 cycle have been simulated. Moreover, two additional driving cycles, New European Driving Cycle (Europe) and Artemis cycle (Europe), have been considered in the work. Finally, a dedicated study to define the DOC size needed to accomplish the different emissions standards is carried out.

2. Materials and methods

2.1. Experimental setup

2.1.1. Engine characteristics

The experiments were carried out on a light-duty, four stroke, single-cylinder diesel engine (SCE) based on a serial production 1.9L platform. The engine has four valves driven by dual overhead cams and equips the serial production piston with re-entrant bowl, which confers a geometric compression ratio of 17.1:1. The SCE has two swirl valves (tangential and helical) in the intake port through which the swirl ratio can be varied from 0 to 5.2, as characterized in a cold flow test rig [36]. In this work, the position of both valves was fixed to give a constant swirl ratio of 1.4 during all the study, which is the lowest value that can be achieved with the stock engine configuration. The main characteristics of the engine are summarized in Table 1.

Table 1. Engine characteristics.

Engine Type	4 stroke, 4 valves, direct injection
Number of cylinders [-]	1
Displaced volume [cm^3]	477
Stroke [mm]	90.4
Bore [mm]	82
Piston bowl geometry [-]	Re-entrant
Compression ratio [-]	17.1:1
Rated power [kW]	27.5 @ 4000 rpm
Rated torque [Nm]	80 @ 2000-2750 rpm

2.1.2. Test cell description

The single-cylinder engine was installed in a test cell with the state-of-the-art subsystems needed for its operation and control. A scheme of the test cell is shown in Figure 1. The desired engine speed and load in the experiments were controlled by means of an electric dynamometer. A screw compressor capable of providing up to 3 bar was used to feed the engine with fresh air. Air relative humidity and temperature were regulated before entering into the intake settling chamber. This settling chamber was sized to attenuate the pulsating nature of the intake flow, thus ensuring a constant air supply to the engine. Pressure and temperature were monitored in the settling chamber for regulation purposes. A high-pressure exhaust gas recirculation (EGR) line was built to recirculate combustion products to the intake manifold. Thus, the intake charge pressure and temperature were monitored again in the intake manifold after the air-EGR mixing. The exhaust pressure and temperature were monitored in the exhaust manifold as well as in the exhaust settling chamber.

The first element of the exhaust line is the DOC. As sketched in Figure 1, pressure and temperature transducers are instrumented at the DOC inlet and outlet. The geometrical parameters of the DOC are listed in Table 2. A five-gas Horiba MEXA-7100 DEGR analyzer was used to measure the gaseous engine-out emissions upwards and downwards the DOC. The measurements in both locations were not done instantaneously. In this case, each operating point was measured three times along a period of 60 seconds with the emissions test probe located upwards the DOC. Later, the same procedure was done with the emissions test probe located downwards the DOC. A settling chamber was installed after the DOC to attenuate the exhaust flow before the EGR bypass. Finally, a pneumatic valve was used to reproduce the backpressure provoked by the turbocharger in the real multi-cylinder engine. Smoke emissions were measured in filter smoke number (FSN) units using an AVL 415S smoke meter. Three consecutive measurements of 1 liter volume each with paper-saving mode off were took at each engine operating point [37].

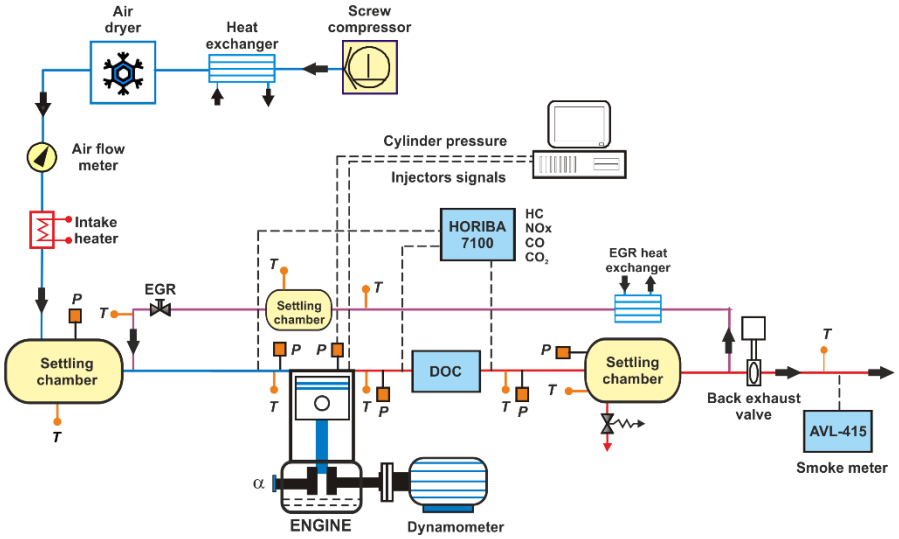

Figure 1. Test cell scheme.

Table 2. Characteristics of the diesel oxidation catalyst used in this work.

Diameter [m]	0.172
Length [m]	0.082
Cell density [cpsi]	400
Cell size [mm]	1.17
Wall thickness [mm]	0.101
Nº of channels	14400
Catalytic area [m^2]	5.5
Specific surface [m^{-1}]	2900
Channel section	Square
Platinum [mol/m^3]	0.3
Zeolite [mol/m^3]	20

The in-cylinder pressure signal was acquired using a Kistler 6125C glow-plug piezoelectric transducer in series with a 4603B10 charge amplifier. 400 consecutive engine cycles were measured at each experimental point. The shaft encoder used provides 720 pulses per revolution, leading to a resolution of 0.5 crank angle degree (CAD). However, a resolution of 0.2 CAD is achieved via interpolation. The pressure data were recorded using a Yokogawa DL708E with a 16 bits A/D converter module. The low frequency variables were acquired at a 100 Hz using an in-house developed recording system named SAMARUC. The accuracy of the main elements of the test cell is shown in Table 3.

Table 3. Accuracy of the instrumentation used in this work.

Variable measured	Device	Manufacturer / model	Accuracy
In-cylinder pressure	Piezoelectric transducer	Kistler / 6125BC	±1.25 bar
Intake/exhaust pressure	Piezorresistive transducers	Kistler / 4603B10	±25 mbar
Temperature in settling chambers and manifolds	Thermocouple	TC direct / type K	±2.5 °C
Crank angle, engine speed	Encoder	AVL / 364	±0.02 CAD
NOx, CO, HC, O_2, CO_2	Gas analyzer	HORIBA / MEXA 7100 DEGR	4%
FSN	Smoke meter	AVL / 415	±0.025 FSN
Gasoline/diesel fuel mass flow	Fuel balances	AVL / 733S	±0.2%
Air mass flow	Air flow meter	Elster / RVG G100	±0.1%

2.1.3. Fuels and injection systems characteristics

RCCI operation was promoted using EN 590 diesel as high reactivity fuel and EN 228 gasoline with 98 RON as low reactivity fuel. The main characteristics of the fuels are depicted in Table 4. To inject both fuels, two fuel injection systems were built using commercial parts. The stock common-rail fuel injection system, with a centrally located solenoid injector, was used to introduce the direct-injected fuel into the cylinder. The injector control was handled through a DRIVVEN control system [40]. The port fuel injection of the low reactivity fuel was done by means of a PFI located at the intake manifold, 160 mm far from the intake valves. The PFI command was done through a Genotec hardware. The PFI timing was set 10 CAD after the intake valve opening (IVO), as this timing showed a proper engine response in a preliminary study. The DI and PFI fuel mass flows were measured using dedicated AVL 733S fuel balances. The main characteristics of the DI and PFI are depicted in Table 5.

Table 4. Physical and chemical properties of the fuels.

	EN 590 diesel	EN 228 gasoline
Density [kg/m^3] (T= 15 °C)	842	747
Viscosity [mm^2/s] (T= 40 °C)	2.929	0.545
RON [-]	-	97.6
MON [-]	-	89.7
Cetane number [-]	51	-
Lower heating value [MJ/kg]	42.50	44.09

Table 5. Characteristics of the direct and port fuel injector.

Direct injector		Port fuel injector	
Actuation Type [-]	Solenoid	Injector Style [-]	Saturated
Steady flow rate @ 100 bar [cm^3/min]	880	Steady flow rate @ 3 bar [cm^3/min]	980
Included spray angle [°]	148	Included Spray Angle [°]	30
Number of holes [-]	7	Injection Strategy [-]	single
Hole diameter [µm]	141	Start of Injection [CAD ATDC]	340
Maximum injection pressure [bar]	1600	Maximum injection pressure [bar]	5.5

2.2. GT drive model

The DOC model is embedded into the GT-drive model to allow the evaluation of the DOC performance on driving cycles representative of different regions and regulations (NEDC, JC08, Artemis, WLTC, FTP 75) and a real driving emissions (RDE) cycle obtained in CMT [38]. The GT drive model was developed for an Opel Vectra that is originally equipped with the engine used in this research. Geometric, aerodynamic and working parameters presented in Table 6 were used as inputs for the model.

Table 6. Vehicle specifications.

Vehicle Mass [kg]	1573
Vehicle Drag Coefficient [-]	0.28
Frontal Area [m^2]	2.04
Tires Size [mm/%/inch]	225/45/R118
Vehicle Wheelbase [m]	2.7
Final Drive Ratio [-]	3.35
Gear Ratio 1^{st} [-]	3.82
Gear Ratio 2^{nd} [-]	2.05
Gear Ratio 3^{rd} [-]	1.3
Gear Ratio 4^{th} [-]	0.96
Gear Ratio 5^{th} [-]	0.74
Gear Ratio 6^{th} [-]	0.61

The final model used in this investigation is illustrated in Figure 2. The experimental performance, engine-out emissions and air mass flow maps were inserted in the engine object whilst the mass fraction and temperature maps at the DOC inlet were allocated in separated arrays. Their values were determined by the instantaneous engine speed and load. These two parameters were obtained according to the instantaneous velocity on the cycle profile. The required velocity value results in a total resistance force that is a sum of vehicle inertia, drag resistance and mechanical losses [39]. With this, it is possible to find the required engine load and engine speed that are needed to achieve the engine velocity and consequently all the information inside the input maps.

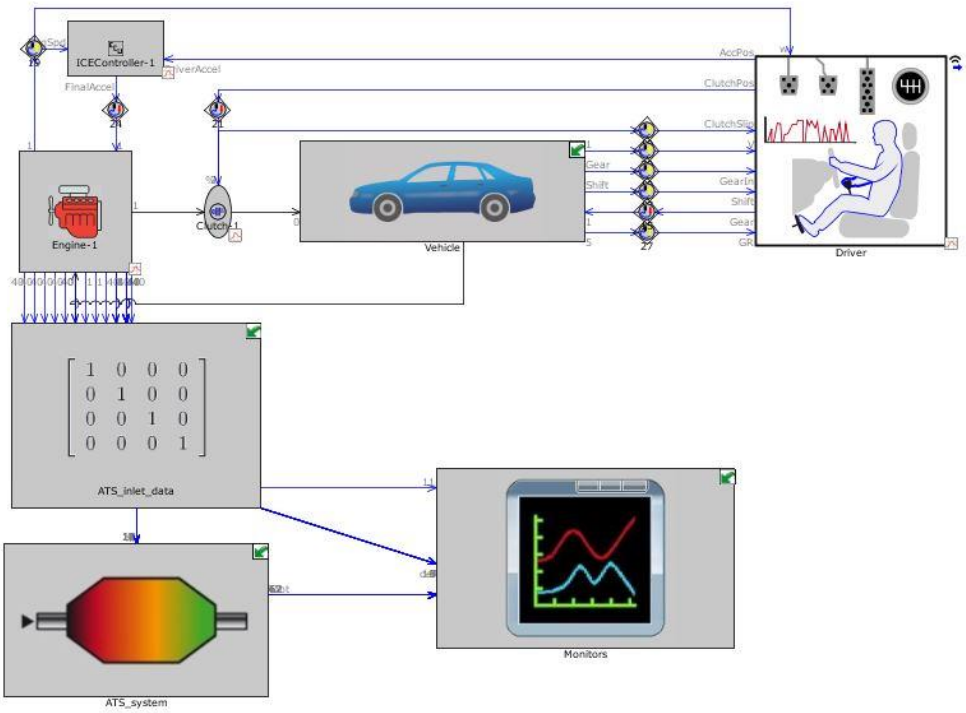

Figure 2. Model developed in GT-drive.

2.3. Modelling procedure

The GT drive simulation tool from Gamma Technologies® was used to model the vehicle in study as well as the aftertreatment system. The following sections are intended to discuss the assumptions, modelling and calibration steps used to obtain the results.

2.3.1. Assumptions

The use of one dimensional simulation approach to assess catalyst performance relies on assumptions related to the flow and temperature field inside the DOC as well as the kinetic mechanism that takes place. They can be listed as follow:

a. The composition of the exhaust HC can be modelled using three representative species: propane, propylene and diesel vapor ($C_{13.5}H_{23.6}$).
b. The reaction mechanism considers global steps of oxidation, absorption and desorption [40].
c. The flow field modelling inside the DOC is based on a quasi-steady approach [41].
d. The water and hydrogen concentrations at the engine exhaust system are determined applying an equilibrium reaction with dissociation considering 11 species [42].
e. For the DOC sizing study, the channel density as well as the material properties are kept the same as the original one.

2.3.2. Hydrocarbon modelling

The real engine-out HC emissions are composed of several species, products of incomplete fuel oxidation in different oxidation routes. Therefore, it can be expected the presence of both small and large HC with different reactivity. Generally, a two-

species approach is applied in conventional DOC models [40]. This method consists of using a high reactivity and a low reactivity HC specie. The most used species for conventional diesel engines are diesel vapor (low reactivity) and propylene (high reactivity). However, RCCI combustion usually presents high levels of gasoline fraction [33]. In this way, it should be included a third specie to describe the low reactivity HC for this fuel (propane). Therefore, in this work they are used three species to model the HC composition: two low reactivity (diesel vapor and propane) and one high reactivity specie, propylene (C_3H_6). The mass percentage of each one was adjusted according to [39]. The composition of each fuel was determined by:

$$Y_{gasoline} = Y_{total\ hydrocarbons} \cdot GF \quad (1)$$

$$Y_{\ diesel} = Y_{total\ hydrocarbon\ } \cdot (1 - GF) \quad (2)$$

Where $GF=m_{gasoline}/(m_{gasoline}+m_{diesel})$. From this moment, each fuel was treated separately and was divided in low and high reactivity species according to GT power manual, as the equations below:

$$Y_{C_3H_{6_G}} = Y_{gasoline} \cdot \%_{HR_G} \quad (3)$$

$$Y_{C_3H_8} = Y_{gasoline} \cdot \%_{LR_G} \quad (4)$$

$$Y_{C_3H_{6_D}} = Y_{diesel} \cdot \%_{HR_D} \quad (5)$$

$$Y_{dieselvap} = Y_{diesel} \cdot \%_{LR_D} \quad (6)$$

Where, G and D stand for gasoline and Diesel and LR and HR stand for low reactivity and high reactivity. Based on this, the final equation representing the exhaust HC composition can be written as:

$$Y_{total\ hydrocarbons\ } = Y_{C_3H_{6_D}} + Y_{C_3H_{6_G}} + Y_{C_3H_8} + Y_{dieselvapour} \quad (7)$$

2.3.3. Boundary conditions and solver settings

Table 7 illustrates the boundary conditions and the settings used in this work. The mass flow, as well as temperature and species concentrations were imposed in the inlet boundary whilst DOC out environment was specified by temperature and pressure conditions. The DOC temperatures as monolith axial temperature distribution and wall temperatures were determined from the balance between convective and diffusive heat transfer taking into account the energy released during the oxidation process. This approach requires the input of the material transport characteristics such as thermal conductivity and heat capacity.

Table 7. Boundary conditions and solver options used in this work.

Boundary conditions	
Inlet-thermal	Dirichlet
Inlet-flow	Mass flow
Outlet-thermal	Dirichlet
Outlet-flow	Pressure
Ambient heat transfer	Robin
Composition	Species mass fraction
Solver options	
Mesh size [adaptive]	Maximum of 800 elements
Flow	Quasi-steady
Thermal	Transient
Step-size	0.001 s
Convergence criteria	10E-6

The chemical reactions were based on the Sampara and Bisset mechanism with species diffusion, adsorption and desorption with an extra route to include propane oxidation [41]. Flow and diffusion were assumed quasi-steady while thermal and chemical evolution were dependent on time. A temporal independence study was performed to determine the maximum time step that is allowed to be used. In addition, the maximum DOC discretization size was evaluated to guarantee independent solution on time-step and space discretization.

3. DOC model calibration

The engine-out emissions measurements were used to calibrate the DOC model. The procedure was performed in two parts. The first one aims to calibrate non-oxidative reactions as adsorption and desorption while the second one is focused on determining the best set of pre-exponential factors (PEF) and energies of activation (Ea) for the oxidation reactions.

3.1. DOC adsorption and desorption calibration

The first phase of the calibration process relied on determining the PEF and Ea for the following reactions:

$$Z + DF \rightarrow ZDF \quad (8)$$

Where DF stands for HC whilst Z stands for zeolite. This first reaction (Equation 8) can be assumed temperature-independent and describes the HC adsorption process by the zeolite. The second reaction complements the mechanism by modelling the HC desorption when its concentration and temperature in zeolites reach a determined level.

$$ZDF \rightarrow Z + DF \quad (9)$$

The experimental tests were performed in a low load condition during 480 s. The experimental and simulated results are depicted in Figure 3. As the time increases, the DOC adsorption capacity decreases, resulting in higher amounts of HC concentrations at the DOC outlet. Figure 3 also shows that there are slight differences between the predicted and experimental values that can be attributed to transient temperature

conditions as well as the simplification of HC species. Despite of this, the total deviation from experiment is lower than 7% for almost all conditions, except for the operating condition at 60 seconds, showing the capability of the model to predict correctly the adsorption and desorption processes.

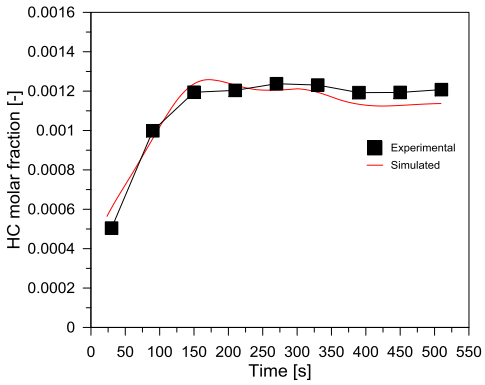

Figure 3. HC transient results: experimental versus simulation results.

3.2. Determination of the pre-exponential factors (PEF) and energies of activation (Ea) for the oxidation reactions

The final stage of the model calibration relies on determining the PEF and Ea for the oxidation reactions. This process presents some difficulties since all the reactions have exponential dependence on the temperature. Therefore, it should be used a large number of operating conditions with different conversion efficiencies. In this sense, 9 operating conditions were measured and both HC and CO conversion efficiency were calculated as shown in Equation 10.

$$Conversion\ efficiency = 100 \cdot \left(\frac{(Y_{inlet} - Y_{outlet})}{Y_{inlet}}\right) \quad (10)$$

Where Y is the mass fraction of the specie under analysis. Table 8 describes each operating condition used during the calibration process.

Table 8. Steady operating conditions used to calibrate the oxidation reactions.

Case	Engine speed [rpm]	IMEP [bar]	EGR [%]	GF [%]	Exhaust T [°C]
1	2000	2	30	50	120
2	2000	1.58	0	58	139.56
3	2000	2.7	23	54	155.15
4	2000	2.83	22	77	174.63
5	3000	2.7	17	53	213.23
6	3000	3.63	32	55	250.33
7	3000	4.6	27	60	271.54
8	3000	5	36	60	288.92
9	3000	6.5	47	64	308.45

Figure 4 presents the comparison between the simulation and experimental results for HC and CO emissions. It can be verified a proper agreement for HC emissions. By contrast, the CO values present significant differences for the cases with exhaust temperatures lower than 180 °C. These points are below the light-off conditions of the catalyst, in which the mechanism used in this work has been found to have a limited

predictive capacity [40]. In these conditions, the HC trend is well captured thanks to using three different HC oxidation reactions, which confers higher flexibility to the model.

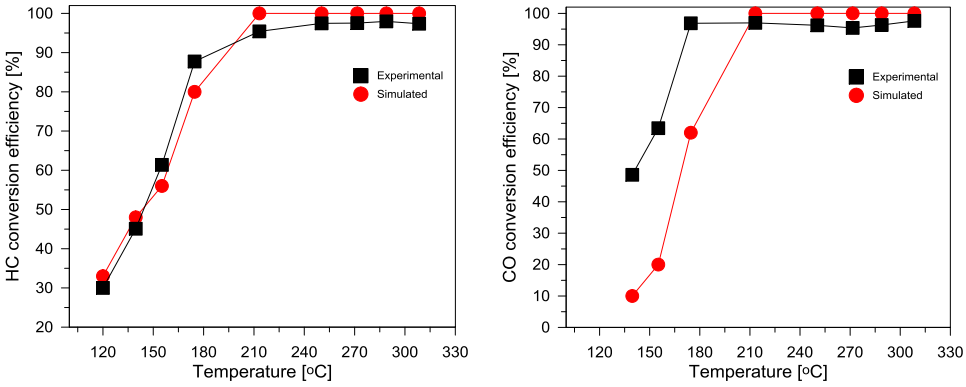

Figure 4. CO and HC results for steady state conditions: experimental *versus* simulated results.

4. Results and discussion

The RCCI regime cannot be used to cover all the engine map, either by excessive HC and CO emissions at very low load or excessive pressure rise rates (PRR) at high loads. By this reason, the dual-mode RCCI/CDC should be implemented. This combustion mode relays on using the RCCI regime whenever possible and cover the rest of the map with CDC, as shown in Figure 5. As it can be seen, the RCCI regime only covers a narrow range inside the whole engine map, representing indicated mean effective pressure (IMEP) values that corresponds to low-medium load conditions.

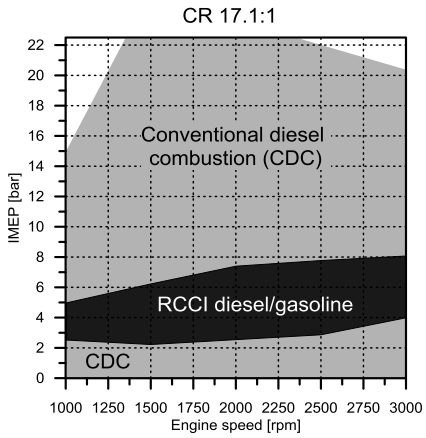

Figure 5. RCCI zone inside the whole engine map.

Six representative driving cycles were studied in this work: Real Driving Emissions cycle (Europe), Worldwide harmonized Light vehicles Test Cycle (Europe), Federal Test Procedure FTP-75 (United States), JC08 (Japan), New European Driving Cycle (Europe) and Artemis cycle (Europe). For the sake of clarity, the results along the paper are explained taking as reference two of the six cycles, and finally, the results of all of them are compared in summary tables (Table 10 and 11). Considering their relevance in Europe, the cycles selected to explain the results are the World Harmonized Light vehicles Test Cycle (WLTC) and a characteristic Real Driving Emissions (RDE) cycle measured by the authors [38]. Figure 6 shows the time-vehicle speed profile of the RDE

cycle and a comparison of the acceleration-velocity conditions found during the NEDC, WLTC and RDE cycles. As it can be seen, the RDE cycle has a greater number of accelerations, including also conditions for engine speeds below 20 km/h, related to city driving.

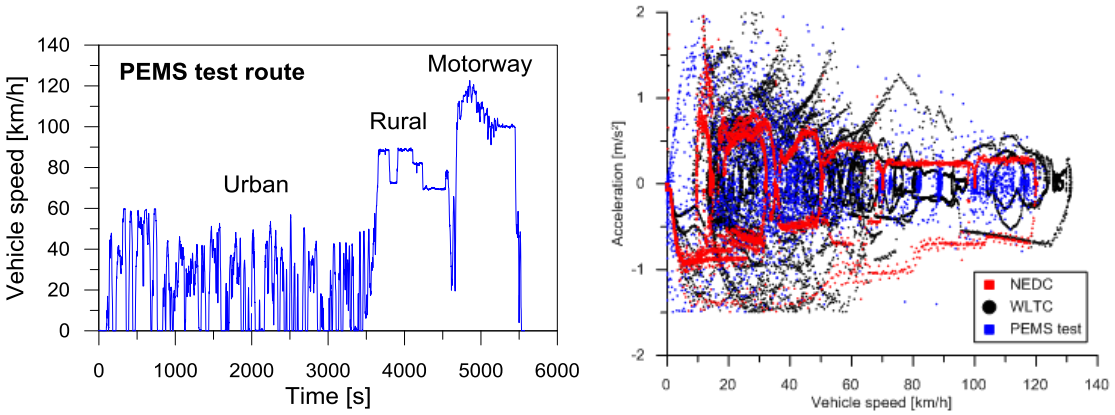

Figure 6. Vehicle speed profile of the RDE cycle (left) and acceleration-velocity conditions for the NEDC, WLTC and RED cycles (right).

Figure 7 shows the ISFC surface map for the dual-mode concept, which is obtained during the bench tests. The symbols plotted over the maps represent some operating conditions reached through the vehicle model simulation along the WLTC (left) and RDE cycle (right). The area defined inside the white dashed lines in the maps represents the RCCI operating region in the global engine map. As it can be seen, in spite of the low region covered by RCCI, the operating conditions covered are quite representative of both driving cycles, which denotes the importance of this combustion mode in the final results.

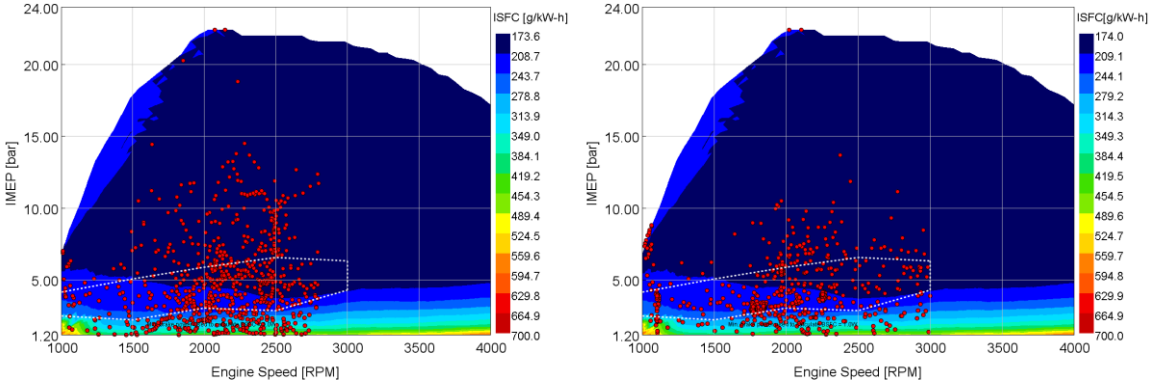

Figure 7. Operating conditions reached during the WLTC cycle (left) and RDE (right). The operating points are represented with red circles. The dashed line limits the RCCI operating region.

Figure 8 summarizes the time percentage spent in each load range during the simulation for the WLTC and RDE cycle. It can be verified that during more than 80 % of the time, the engine load is below 6.4 bar of IMEP, i.e., conditions in which the RCCI regime prevails. As literature demonstrates, RCCI leads to simultaneous ultra-low NOx and soot emissions. However, huge amounts of HC a CO are emitted as result of the low combustion efficiency [43]. Based on this, it is necessary to evaluate the original after treatment system to verify its capability to deal with the high amounts of HC and CO emissions from the RCCI combustion.

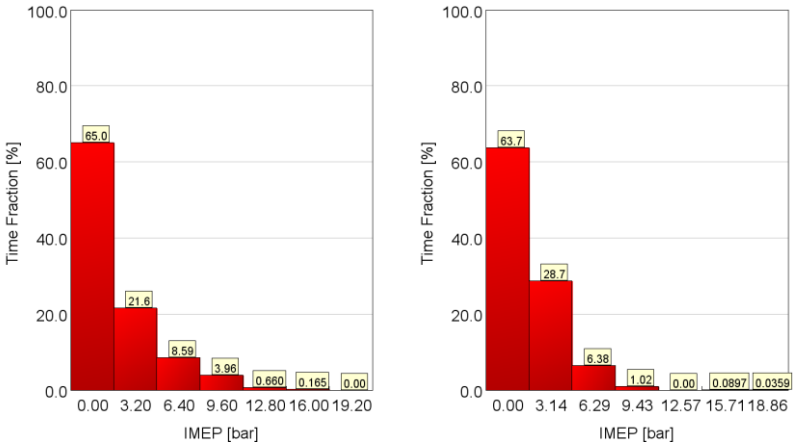

Figure 8. Time fraction spent in each load zone for WLTC (left) and RDE (right).

4.1. Estimations of the DOC efficiency in transient conditions

It is possible to perform a reverse analysis using the instantaneous IMEP and engine speeds values achieved during the driving cycle. This allows determining if the emission comes from the RCCI or CDC condition. With this, the total HC and CO amount can be separated according each combustion mode allowing to quantify their importance in the final emissions. The results of this analysis for the WLTC are presented in Figure 9.

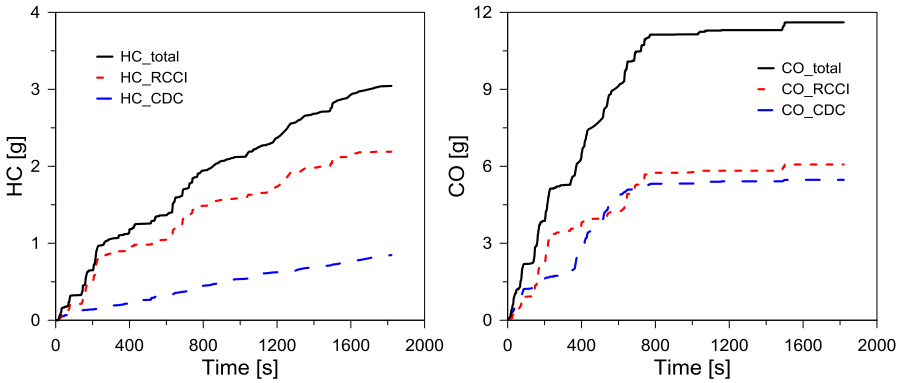

Figure 9. Cumulative HC and CO emissions at the DOC outlet separated by its source (RCCI or CDC combustion) during the WLTC driving cycle.

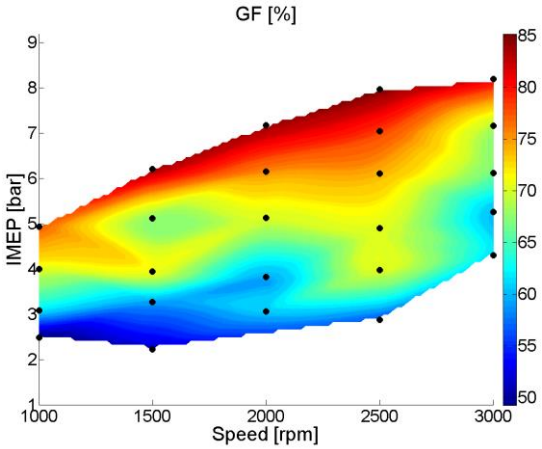

Figure 10. GF used in the RCCI portion of the map.

From Figure 9, it is possible to verify that almost all the HC emissions come from RCCI operation mode, which are mainly composed of gasoline (Figure 10). The increase of the HC concentration reaching the DOC wall difficults a proper conversion of this specie. In the DOC model, the HC from RCCI is mainly composed of propane since this specie was used as a low reactivity specie for gasoline incomplete combustion. The energy of activation required to the oxidation reaction of propane may be higher compared to the one required by the propylene and diesel vapor. Therefore, the complete oxidation of this specie is not reached resulting in high amounts of unburned HC in the DOC outlet. Nonetheless, the CO outlet value seems to depend equally on RCCI and CDC modes since it is the same molecule for both combustion modes. In addition, the conversion reactions start at lower temperatures. Therefore, it main dependency relies on the oxygen concentration at the DOC inlet to provide the reactants to the reaction takes place.

In this way, the final map containing the RCCI zone was assessed for the aforementioned driving cycles to evaluate the possibility of operating with the original vehicle setup. The results of each driving cycle are presented in Figure 11, where the blank bars inform the normative limits, and the filled bars are the DOC-in and DOC-out values of HC and CO emissions in g/km. The RDE and WLTC are presented with Euro 6 limits while NEDC and Artemis are related to the Euro 4. The JC08 cycle results are compared with its respective normative. In the case of FTP-75, there is no direct limit to unburned HC. Therefore, for this research the values of Euro 6 were used as reference. Most of the actual emissions regulations presents limits for the total HC+NO_x emissions, NOx, CO and Soot. Thus, in order to allow an analysis addressing only the HC emissions, it was considered that the engine has a NOx aftertreatment system able to reduce this emissions up to the maximum legislation level. In this way, the NOx limit can be subtracted in the NOx+HC limit, resulting in the required value for the HC emissions at the DOC outlet.

As Figure 11 shows, none of the simulated cases was able to obtain values inside the type approval regulation limit. The higher amount of HC and CO produced compared to the conventional diesel combustion considerably increases the DOC out emissions. Since the oxidation reaction for these two species takes place in the same sites, they are always competing, which inhibits the oxidation reactions at some extent [44]. In addition, the exhaust temperature for the RCCI case is lower than the CDC resulting in slower reaction rates. Therefore, the conversion efficiency for the cycle conditions that are inside the RCCI zone are worsened, making impossible to achieve the required normative values.

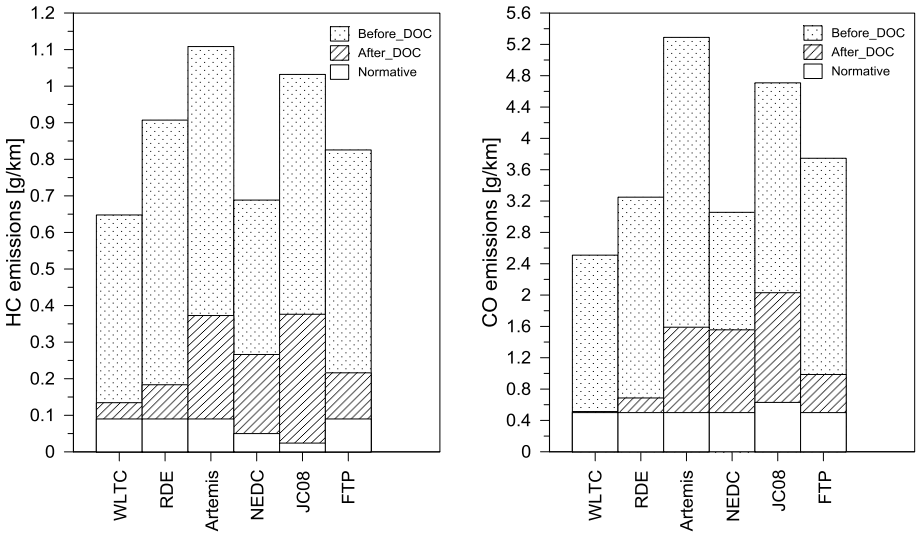

Figure 11. After and before DOC distance averaged final emissions and normative values for each cycle.

4.2. DOC sizing study

Since the original DOC is not able to achieve the emissions levels proposed by the emissions regulations, a sizing study is proposed to determine the required volume to reach the normative values for HC and CO. This will serve to evaluate the conversion efficiency dependency with respect to the DOC size. Because of the novelty and the increasing interest of the RDE cycle in Europe, it was selected to perform the DOC sizing. Since the RDE is a complementary cycle of the WLTC, the later has been also analyzed in this study. It is worth to state that only the DOC volume was changed. Therefore, it was not taken into account any possible improvement on materials, channel geometry and its density. Table 9 describes the different volumes tested in the sizing study.

Table 9. Operating conditions tested in respect to the DOC volume.

Case number	V/Vo ratio [-]	Total DOC Volume [L]
Case 1	1/4	0.475
Case 2	1/2	0.95
Case 3	1	1.9
Case 4	2	3.8
Case 5	4	7.6
Case 6	6	11.4

From Figure 12, it can be inferred that the HC emissions have a dominant role on the DOC size, i.e., the DOC size should be designed looking to the HC emissions. For the WLTC driving cycle, only volumes higher than 3 times are able to obtain values closer to the normative ones. It is also possible to verify that both species have an exponential decay as the volume is increased. Therefore, volume steps towards higher volumes results in small changes in the DOC outlet species mass. This behavior is attributed to the higher heat transfer rates to the ambient, since that, the total area considerably increases. Regarding the CO, it is required volumes between the original and two times the original DOC volume to fulfill the normative values for this driving cycle.

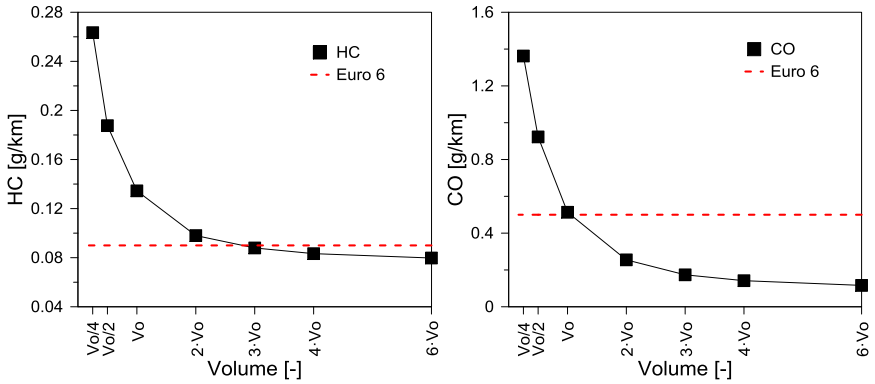

Figure 13. HC and CO emissions for WLTC driving cycle for different DOC volumes and Euro 6 limits respectively.

Due to the higher cycle duration and the larger amount of the operating conditions inside the RCCI zone, it was not possible to obtain values under Euro 6 emissions for the DOC size of 4 times the initial volume. As seen in Figure 13, the normative constraint was only achieved for a volume between four and six times the initial volume.

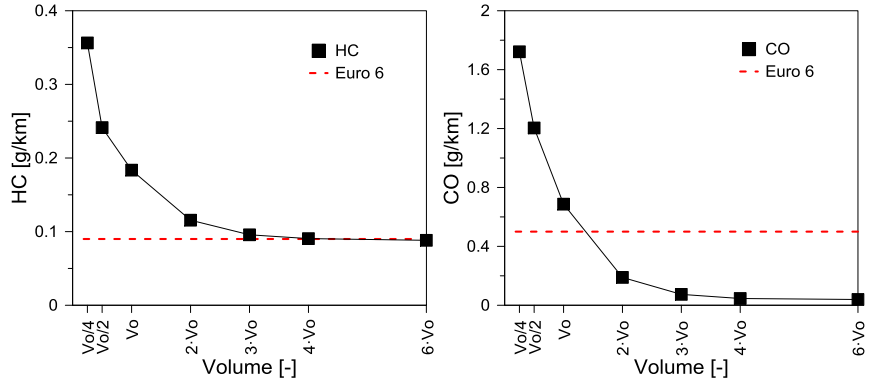

Figure 13. HC and CO emissions for RDE driving cycle for different DOC volumes and Euro 6 limits respectively.

The summary of the results obtained for all the driving cycles evaluated are presented in Table 10 and Table 11, where is possible to verify the normative values for the HC and CO emissions and the values obtained at the DOC inlet and outlet. From the tables, it can be inferred that the addition of RCCI combustion mode results in an increase in the DOC load requiring a higher volume to reduce the HC and CO emissions to normative levels. From Table 10, it can be inferred that the increase in the size volume to meet the limits proposed by the different regulations ranges from four to six times the original volume. Comparing both emission species, it can be seen that HC emissions are more restrictive, requiring a higher DOC volume to reduce the emissions down to the regulation levels, except for the NEDC. Comparing among the different driving cycles, it is clear that the JC08 cycle is the most restrictive one, fulfilling the CO limits with a DOC volume of $6 \cdot V_0$, but not achieving the HC limits in any case. The WLTC is fulfilled with $3 \cdot V_0$, while the RDE cycle requires $4 \cdot V_0$, which confirms its severity as compared to WLTC. The FTP-75 is the second most restrictive, requiring using a DOC of $6 \cdot V_0$. Finally, the Artemis cycle requires $3 \cdot V_0$ and the NEDC requires $6 \cdot V_0$ due to the CO emissions.

Table 10. Summary table for HC emission addressing all the driving cycles tested in the study.

	Eu6			American		Eu4			Japanese	
Volume	**WLTC [g/km]**	**RDE [g/km]**	**Limits [g/km]**	**FTP 75 [g/km]**	**Limits [g/km]**	**NEDC [g/km]**	**Artemis [g/km]**	**Limits [g/km]**	**JC08 [g/km]**	**Limits [g/km]**
6.Vo	**0.08**	**0.09**		**0.09**		**0.13**	**0.16**		0.17	
4.Vo	**0.08**	**0.09**		0.10		**0.15**	**0.17**		0.19	
3.Vo	**0.09**	0.10		0.10		**0.18**	**0.18**		0.20	
2.Vo	0.10	0.12	**0.09**	0.13	**0.09**	**0.22**	0.23	**0.22**	0.27	**0.024**
Vo	0.13	0.18		0.22		0.27	0.37		0.38	
Vo/2	0.19	0.24		0.31		0.31	0.55		0.50	
Vo/4	0.26	0.36		0.41		0.38	0.69		0.62	

Table 11. Summary table for CO emission addressing all the driving cycles tested in the study.

	Eu6			American		Eu4			Japanese	
Volume	**WLTC [g/km]**	**RDE [g/km]**	**Limits [g/km]**	**FTP 75 [g/km]**	**Limits [g/km]**	**NEDC [g/km]**	**Artemis [g/km]**	**Limits [g/km]**	**JC08 [g/km]**	**Limits [g/km]**
6.Vo	**0.12**	**0.04**		**0.05**		**0.43**	**0.25**		**0.44**	
4.Vo	**0.14**	**0.05**		**0.06**		0.56	**0.29**		0.57	
3.Vo	**0.17**	**0.07**		**0.09**		0.73	**0.38**		0.73	
2.Vo	**0.25**	**0.19**	**0.50**	**0.27**	**0.50**	1.03	0.66	**0.50**	1.19	**0.63**
Vo	0.51	0.69		0.99		1.56	1.59		2.03	
Vo/2	0.92	1.20		1.86		2.06	3.01		3.26	
Vo/4	1.36	1.72		2.50		2.43	4.32		3.94	

5. Conclusions

This paper evaluated the performance of a conventional Diesel oxidation catalyst working under both RCCI and CDC combustion modes and its respective resizing to fulfill the regulation limits for different driving cycles. Initially, values of DOC outlet emissions for the original dimensions were obtained and compared with the limits. Despite of the narrow range of RCCI in the total map, it was verified that it has the major importance on the final HC emissions. The high amounts of HC competing with the CO oxidation leaded to excessive final values of these emissions at the DOC outlet, requiring a resizing study to allow the operation at emissions levels lower than the normative ones. For this, volumes ranging from Vo/4 to 6·Vo were evaluated for six different driving cycles to obtain a general size that attain normative values for the most used regulations. The results demonstrated that the DOC volume needed to fulfill the type approval regulation limits ranges from four to six times the original volume. This can results in packing, weight and construction issues. Therefore, alternative solutions should be investigated, aiming to achieve higher conversion efficiencies with lower volumes. Among them, the modification of wash coat material and covering should be addressed in future works as well as modifications of channel number and geometry.

Acknowledgments

The authors gratefully acknowledge General Motors Global Research & Development for providing the engine used in this investigation. The authors also acknowledge FEDER and Spanish Ministerio de Economía y Competitividad for partially supporting this research through TRANCO project (TRA2017-87694-R).

References

[1] Araghi Y, Kroesen M, Van Wee B. Identifying reasons for historic car ownership and use and policy implications: An explorative latent class analysis. Transport Policy, Volume 56, May 2017, Pages 12-18.

[2] González J, Otsuka Y, Araki M, Shiga S. Impact of new vehicle market composition on the light-duty vehicle fleet CO2 emissions and cost. Energy Procedia, Volume 105, May 2017, Pages 3862-3867.

[3] Fontaras G, Dilara P. The evolution of European passenger car characteristics 2000–2010 and its effects on real-world CO2 emissions and CO2 reduction policy. Energy Policy, Volume 49, October 2012, Pages 719-730.

[4] Garcia A, Monsalve-Serrano J, Heuser B, Jakob M, Kremer F, Pischinger S. Influence of fuel properties on fundamental spray characteristics and soot emissions using different tailor-made fuels from biomass. Energy Conversion and Management, Volume 108, 15 January 2016, Pages 243-254.

[5] Serrano JR, Bermudez V, Piqueras P, Angiolini E. Application of Pre-DPF Water Injection Technique for Pressure Drop Limitation. SAE Technical Paper 2015-01-0985. https://doi.org/10.4271/2015-01-0985.

[6] Ettireddy PR, Kotrba A, Spinks T, Boningari T, Smirniotis P. Development of Low Temperature Selective Catalytic Reduction (SCR) Catalysts for Future Emissions Regulations. SAE Technical Paper 2014-01-1520. https://doi.org/10.4271/2014-01-1520.

[7] Yamauchi T, Takatori Y, Fukuda K. Experimental and Numerical Analysis for a Urea-SCR Catalytic Converter. SAE Technical Paper 2016-01-0973. https://doi.org/10.4271/2016-01-0973.

[8] Singh N, Rutland C, Foster D, Narayanaswamy K, He Y. Investigation into Different DPF Regeneration Strategies Based on Fuel Economy Using Integrated System Simulation. SAE Technical Paper 2009-01-1275. https://doi.org/10.4271/2009-01-1275.

[9] Bhardwaj OP, Krishnamurthy K, Blanco-Rodriguez D, Holderbaum B. Comparative Study to Assess the Potential of Different Exhaust Gas Aftertreatment Concepts for Diesel Powered Ultra-Light Commercial Vehicle Applications in View of Meeting BS VI Legislation. SAE Technical Paper 2017-26-0128. https://doi.org/10.4271/2017-26-0128.

[10] García-Valladolid P, Tunestal P, Monsalve-Serrano J, García A, Hyvönen J. Impact of diesel pilot distribution on the ignition process of a dual fuel medium speed marine engine. Energy Conversion and Management, Volume 149, 1 Oct 2017, Pages 192-205.

[11] Yanagihara H, Sato Y, Minuta J. A simultaneous reduction in NOx and soot in diesel engines under a new combustion system (Uniform Bulky Combustion System e UNIBUS). In: 17th International Vienna motor symposium; 1996.-14-303, 1996.

[12] Wu HW, Wang RH, Ou DJ, Chen YC, Chen TY. Reduction of smoke and nitrogen oxides of a partial HCCI engine using premixed gasoline and ethanol with air. Applied Energy 2011-90-80, 2011.
[13] Koci C, Ra Y, Krieger R, Andrie M, et al. Detailed Unburned Hydrocarbon Investigations in a Highly-Dilute Diesel Low Temperature Combustion Regime. SAE Int. J. Engines 2(1):858-879, 2009, doi:10.4271/2009-01-0928.
[14] Harada A, Shimazaki N, Sasaki S. The effects of mixture formation on premixed lean diesel combustion. SAE Tech Pap 1998, 980533.
[15] Jin Kusaka, Takashi Okamoto, Yasuhiro Daisho, Ryouji Kihara, Takeshi Saito, Combustion and exhaust gas emission characteristics of a diesel engine dual- fueled with natural gas, JSAE Review, Volume 21, Issue 4, October 2000, Pages 489-496, ISSN 0389-4304, http://dx.doi.org/10.1016/S0389-4304(00)00071-0.
[16] Kokjohn S L, Hanson R M, Splitter D A, Reitz R D. Fuel reactivity controlled compression ignition (RCCI): a pathway to controlled high-efficiency clean combustion, International Journal of Engine Research, 2011. Volume 12, June 2011, Pages 209-226.
[17] Inagaki K, Fuyuto T, Nishikawa K, Nakakita K, Sakata I. Dual-Fuel PCI Combustion Controlled by In-Cylinder Stratification of Ignitability. SAE Technical Paper 2006-01-0028, 2006.
[18] Benajes J, Molina S, García A, Monsalve-Serrano J. Effects of low reactivity fuel characteristics and blending ratio on low load RCCI (reactivity controlled compression ignition) performance and emissions in a heavy-duty diesel engine. Energy, Volume 90, October 2015, Pages 1261–1271.
[19] Ryskamp R, Thompson G, Carder D and Nuszkowski J. The Influence of High Reactivity Fuel Properties on Reactivity Controlled Compression Ignition Combustion. SAE Technical Paper 2017-24-0080, 2017.
[20] Li Y, Jia M, Chang Y, Xie M, Reitz R. Towards a comprehensive understanding of the influence of fuel properties on the combustion characteristics of a RCCI (reactivity controlled compression ignition) engine. Energy, Volume 99, March 2016, Pages 69-82.
[21] Benajes J, Molina S, García A, Monsalve-Serrano J. Effects of Direct injection timing and Blending Ratio on RCCI combustion with different Low Reactivity Fuels. Energy Conversion and Management, Volume 99, July 2015, Pages 193-209.
[22] Yang Y, Dec J, Dronniou N, Sjöberg M. Tailoring HCCI heat-release rates with partial fuel stratification: Comparison of two-stage and single-stage-ignition fuels. Proceedings of the Combustion Institute, Volume 33 (2), pp. 3047-3055, 2011.
[23] Li B, Li Y, Liu H, Liu F, Wang J. Combustion and emission characteristics of diesel engine fueled with biodiesel/PODE blends. Applied Energy, Volume 206, 15 November 2017, Pages 425-431.
[24] Curran S, Hanson R, Wagner R. Reactivity controlled compression ignition combustion on a multi-cylinder light-duty diesel engine. International Journal of Engine Research 13 (3), 216-225.
[25] Benajes J, García A, Pastor JM, Monsalve-Serrano J. Effects of piston bowl geometry on Reactivity Controlled Compression Ignition heat transfer and combustion losses at different engine loads. Energy, Volume 98, March 2016, Pages 64-77.

[26] Benajes J, García A, Monsalve-Serrano J, Balloul I, Pradel G. Evaluating the reactivity controlled compression ignition operating range limits in a high-compression ratio medium-duty diesel engine fueled with biodiesel and ethanol. International Journal of Engine Research, Volume 18 (1-2), Pages 66-80, 2017.

[27] Park S, Shin D, Park J. Effect of ethanol fraction on the combustion and emission characteristics of a dimethyl ether-ethanol dual-fuel reactivity controlled compression ignition engine. Applied Energy, Volume 182, November 2016, Pages 243-252.

[28] Benajes J, Pastor JV, García A, Boronat V. A RCCI operational limits assessment in a medium duty compression ignition engine using an adapted compression ratio. Energy Conversion and Management, Volume 126, 2016, Pages 497-508.

[29] Yang B, Yao M, Cheng W, Li Y, Zheng Z, Li S. Experimental and numerical study on different dual-fuel combustion modes fuelled with gasoline and diesel. Appl Energy, 113 (2014), pp. 722–733.

[30] Li J, Yang W, Goh T, An H, Maghbouli A. Study on RCCI (reactivity controlled compression ignition) engine by means of statistical experimental design. Energy, 78, pp. 777–787, 2014.

[31] Benajes J, García A, Monsalve-Serrano J, Boronat V. An investigation on the particulate number and size distributions over the whole engine map from an optimized combustion strategy combining RCCI and dual-fuel diesel-gasoline. Energy Conversion and Management, Volume 140, 15 May 2017, Pages 98-108.

[32] Benajes J, García A, Monsalve-Serrano J, Balloul I, Pradel G. An assessment of the dual-mode reactivity controlled compression ignition/conventional diesel combustion capabilities in a EURO VI medium-duty diesel engine fueled with an intermediate ethanol-gasoline blend and biodiesel. Energy Conversion and Management, Volume 123, July 2016, Pages 381-391.

[33] Benajes J, García A, Monsalve-Serrano J, Boronat V. Achieving clean and efficient engine operation up to full load by combining optimized RCCI and dual-fuel diesel-gasoline combustion strategies. Energy Conversion and Management, Volume 136, 15 March 2017, Pages 142-151.

[34] Benajes J, García A, Monsalve-Serrano J, Villalta D. Exploring the limits of the RCCI combustion concept in a light-duty diesel engine and the influence of the direct-injected fuel properties. Energy Conversion and Management, Volume 157, 2018, Pages 277-287.

[35] García A, Monsalve-Serrano J, Rückert Roso V, Santos Martins M. Evaluating the emissions and performance of two dual-mode RCCI combustion strategies under the World Harmonized Vehicle Cycle (WHVC). Energy Conversion and Management, Volume 149, 1 Oct 2017, Pages 263-274.

[36] Olmeda P, Martin J, Garcia A, Villalta D, Warey A, Domenech V. A Combination of Swirl Ratio and Injection Strategy to Increase Engine Efficiency. SAE International Journal of Engines 10(3):2017, doi:10.4271/2017-01-0722

[37] AVL manufacturer manual. Smoke value measurement with the filter-papermethod. Application notes. June 2005 AT1007E, Rev. 02. Web:<https://www.avl.com/documents/10138/885893/Application+Notes >.

[38] Luján JM, Bermúdez V, Dolz V, Monsalve-Serrano J. An assessment of the real-world driving gaseous emissions from a Euro 6 light-duty diesel vehicle using a

portable emissions measurement system (PEMS). Atmospheric Environment, Volume 174, Feb 2018, Pages 112-121.
[39] Gamma Technologies: Vehicle Driveline and HEV Application Manual. 2018.
[40] Sampara C, Bissett E, Chmielewski M. Global Kinetics for a Commerical Diesel Oxidation Catalyst with Two Exhaust Hydrocarbons. Industrial Engineering and Chemical Research, Volume 47, 18 December 2008, Pages 311-322.
[41] Sampara C, Bissett E, Chmielewski M, Assanis D. Global Kinetics for Platinum Diesel Oxidation Catalysts. Industrial & Engineering Chemistry Research, Volume 46, 6 October 2007, Pages 7993-8003.
[42] Silvis W. An Algorithm for Calculating the Air/Fuel Ratio from Exhaust Emissions. SAE Technical Paper 970514, 1997.
[43] Desantes JM, Benajes J, García A, Monsalve-Serrano J, The Role of the In-Cylinder Gas Temperature and Oxygen Concentration over Low Load RCCI Combustion Efficiency. Energy, Volume 78, 15 December 2014, Pages 854–868.
[44] Al-Harbi M, Hayes R, Votsmeier M, Epling W. Competitive NO, CO and hydrocarbon oxidation reactions over diesel oxidation catalyst. The Canadian Journal of Chemical Engineering, Volume 90, December 2012, Pages 1527-1538.

Abbreviations

ATDC: After Top Dead Center

CAD: Crank Angle Degree

CDC: Conventional Diesel Combustion

CI: Compression Ignition

CO: Carbon Monoxide

CR: Compression Ratio

DI: Direct Injection

DPF: Diesel Particulate Filter

EGR: Exhaust Gas Recirculation

Ea: Energy of Activation

FSN: Filter Smoke Number

FTP: Federal Test Procedure

GF: Gasoline Fraction

HC: Hydro Carbons

HCCI: Homogeneous Charge Compression Ignition

HRF: High Reactivity Fuel

IMEP: Indicated Mean Effective Pressure

IVO: Intake Valve Open

LRF: Low Reactivity Fuel

LTC: Low Temperature Combustion

MPRR: Maximum Pressure Rise Rate

NOx: Nitrogen Oxides

ON: Octane Number

PEF: Pre-exponential Factor

PFI: Port Fuel Injection

PPC: Partially Premixed Charge

PRR: Pressure Rise Rate

RCCI: Reactivity Controlled Compression Ignition

RDE: Real Driving Emissions

SCE: Single Cylinder Engine

SCR: Selective Catalytic Reduction

WLTC: Worldwide harmonized light vehicles Test Cycle